JACS
JOURNAL OF THE AMERICAN CHEMICAL SOCIETY
Article
pubs.acs.org/JACS

Metal-Induced Conformational Changes of Human Metallothionein-2A: A Combined Theoretical and Experimental Study of Metal-Free and Partially Metalated Intermediates

Shu-Hua Chen, Liuxi Chen, and David H. Russell*

Department of Chemistry, Texas A&M University, College Station, Texas 77843, United States

Supporting Information

ABSTRACT: Electrospray ionization ion mobility mass spectrometry (ESI IM-MS) and molecular dynamics (MD) simulations reveal new insights into metal-induced conformational changes and the mechanism for metalation of human metallothionein-2A (MT), an intrinsically disordered protein. ESI of solutions containing apoMT yields multiple charge states of apoMT; following addition of Cd^{2+} to the solution, ESI yields a range of Cd_iMT (i = 1−7) product ions (see Chen et al. *Anal. Chem.* **2013**, *85*, 7826−33). Ion mobility arrival-time distributions (ATDs) for the Cd_iMT (i = 0−7) ions reveal a diverse population of ion conformations. The ion mobility data clearly show that the conformational diversity for apoMT and partially metalated ions converges toward ordered, compact conformations as the number of bound Cd^{2+} ions increase. MD simulations provide additional information on conformation candidates of Cd_iMT (i = 0−7) that supports the convergence of distinct conformational populations upon metal binding. Integrating the IM-MS and MD data provides a global view that shows stepwise conformational transition of an ensemble as a function of metal ion bound. ApoMT is comprised of a wide range of conformational states that populate between globular-like compact and coil-rich extended conformations. During the initial stepwise metal addition (number of metal ions bound i = 1−3), the metal ions bind to different sites to yield distinct conformations, whereas for i > 4, the conformational changes appear to be domain-specific, attributed to different degrees of disorder of the β domain; the β domain becomes more ordered as additional metal ions are added, promoting convergences to the dumbbell-shaped conformation.

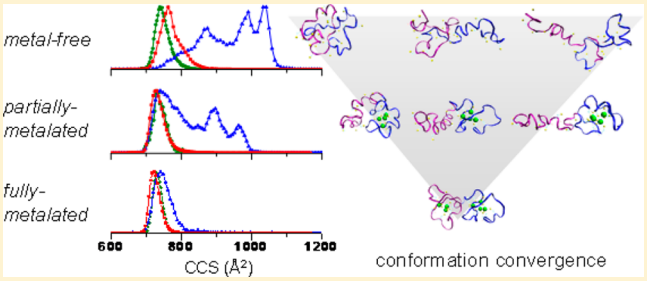

INTRODUCTION

One-third of proteins naturally bind metal ions in order to provide activity and/or stability.[1] Aberrant metalation has been linked to protein misfolding and human disease, specifically pathogenic processes of amyloidosis, including Aβ-peptide aggregation in Alzeheimer's disease (AD), α-synuclein in Parkinson's disease (PD), and prion protein in transmissible spongiform encephalopathies (TSE).[2] There is increasing evidence that Cu^{2+} ions disrupt Aβ-peptide from adapting a β-sheet conformation,[3,4] and that Cu^{2+} and Fe^{3+} ions trigger structural transformations as well as increases in the fibrillation rate of α-synuclein.[5] Similarly, Zn^{2+} and Cu^{2+} ions alter prion protein aggregation pathways and lead to formation of amorphous aggregates instead of fibrils.[6] Not surprisingly, however, metal−protein interactions also have potential in the development of therapeutic agents. For example, Mg^{2+} inhibits α-synuclein aggregation,[7] and binding of Zn^{2+} to Aβ-peptide reduces cytotoxicity.[8] Metallothioneins (MTs), a class of metalloproteins, are known as one of the most important *in vivo* metal reservoirs and transporters.[9,10] MTs are cysteine-rich and possess diverse metal binding preferences that serve to regulate essential metal ions and offer protection against toxicity of non-essential metal ions.[11,12] It is becoming increasingly evident that MTs play protective roles in neurodegenerative diseases by buffering free zinc in amyotrophic lateral sclerosis (ALS)[13] and reducing copper toxicity and production of reactive oxygen species (ROS) in AD.[14,15] MTs are also free-radical scavengers and protect against nephrotoxicity from Cd^{2+} exposure.[11,16] In addition, MTs have been found substantially unsaturated with metal ions in many tumors,[17] and recent evidence suggests that the metal-unsaturated MTs are biologically active in terms of cellular metal metabolism and redox balance.[18,19] Despite the roles of MTs in various diseases, the underlying mechanisms regarding the role of metal ions in promoting protein conformational changes as well as influencing subsequent chemical/biological pathways are poorly understood.

It is generally accepted that the structures of MTs are determined by the number and type of metal ions they coordinate.[12] Structure determination of MTs has proved to be a real challenge owing to their dynamical conformations that make crystallization difficult—impossible in most cases.[12] A major step forward in understanding the chemical/biological properties of MTs was the determination of the atomic-level structure of fully metalated MTs by integrating structural

Received: May 13, 2014
Published: June 11, 2014

   dx.doi.org/10.1021/ja5047878 | *J. Am. Chem. Soc.* 2014, 136, 9499−9508

information from an X-ray crystal structure (rat MT-2A) by Stout et al.[20] and from NMR structures (rat, rabbit, and human MT-2A) by Wüthrich et al.[21−23] They assigned a dumbbell-shaped three-dimensional structure to human Cd_7MT-2A protein comprising two distinct metal binding domains denoted as $Cd_3\beta$- and $Cd_4\alpha$-domains.[21,24] Despite the success in structure determination of fully metalated MTs, there is increasing evidence that apo and partially metalated species are physiologically abundant and may also have important biological roles.[18,19] However, further structural characterization of these metal-unsaturated species has encountered a bottleneck. Blindauer noted that apo and partially metalated MTs are likely to be unfolded to some degree, and thus not amenable to traditional structural studies such as X-ray crystallography.[12] In addition, many biophysical techniques commonly used for characterization of protein conformation are limited to well-defined systems, i.e., solutions of pure protein or high-quality crystals. Unfortunately, dynamic equilibria between apo and partially metalated forms present a significant challenge in terms of isolation of individual metalated states from a complex protein pool. Previous mass spectrometry (MS) studies have shown that more than six metalation states of Cd_iMT (or Zn_iMT; i = 0−7) coexist in solution,[25−28] and multiple structural conformers for each metalated state add an additional layer of complexity. Because traditional biophysical techniques measure the average response for the entire system, it is difficult or even impossible to resolve signals derived from a single conformer in the presence of other closely related conformers from a single metalated state, let alone in the presence of multiple metalated states. In addition, attempts at elucidating structural transitions associated with metal binding by circular dichroism (CD) and optical methods such as UV/vis and fluorescence are generally ineffective because mammalian MTs lack well-defined secondary structure and do not contain aromatic amino acids.[12] Fluorescence resonance energy transfer analysis utilizing labeling at two termini provides information about the change in the distance between the two sensors,[29−31] and dynamic light scattering[32] and small-angle X-ray scattering provide information about particle size distribution. However, such studies also measure the population-averaged responses and do not provide molecule-specific information, which limits the information content to comparisons between metal-free and fully metalated states. Therefore, after nearly six decades of MT research, the only 3-D molecular characterization technique for studies of apo and partially metalated species has been molecular modeling,[12] and comparable experimental evidence has been lacking. Consequently, questions concerning the conformational micro-heterogeneity of the apo and partially metalated species or how the distribution of conformations changes as a result of metal accumulation remain unanswered, and the metalation mechanism remains unclear.

Fenselau and co-workers pioneered the application of electrospray ionization mass spectrometry (ESI-MS) for studying MTs.[27,33−36] ESI-MS is now increasingly used for studies of complex biological samples; there is increasing evidence that, under well-controlled conditions, native-like conformations of proteins can be retained during the ESI process.[37−39] In our previous study, a combination of chemical labeling and top-down and bottom-up proteomic ESI-MS provided valuable new insights into the metalation/demetalation of the human metallothionein MT-2A.[28] The study revealed that (1) metalation of MT by Cd^{2+} occurs by a stepwise mechanism, as originally suggested by Winge;[40] (2) partially metalated Cd_4MT is a relatively stable intermediate, as supported by a sharp increase in stepwise apparent association constant; and (3) all Cd^{2+} ions are located in the α domain for Cd_4MT.[28] Although the study provided a new level of understanding of the metalation mechanism and new experimental approaches for probing the apparent association constant and location of the bound metal ion, structures of the metalated species remain unclear.

Ion mobility mass spectrometry (IM-MS) has emerged as a promising approach for characterization of protein conformation, and Guo et al. have reported IM-MS results for apo- and fully metalated Cd_7MT.[41] Here, IM-MS is employed to investigate stepwise conformational changes of human MT-2A as a function of the number of Cd^{2+} ions bound. IM-MS provides an unparalleled approach for monitoring all the distinct MT conformers owing to its unique capabilities for (1) separation of the multiple metalated states, i.e., the initial apoprotein, intermediates inherent to the metalation reactions, and the final products, on the basis of their characteristic m/z ratios by mass spectrometry, and (2) interrogation of the conformer population for individual metalation states. Molecular dynamics (MD) simulations are used to generate protein conformations whose collision cross section (CCS) can be correlated to the experimental IM-MS CCS. We show here the first experimental data for conformational populations of each of the metalated forms. The integrated IM-MS and MD approach offers a global view of the conformational changes that occur upon metal binding and provides new insights into the metalation mechanism.

EXPERIMENTAL SECTION

Materials. Recombinant human metal-free MT-2A (apoMT) was obtained from Bestenbalt LLC (Tallinn, Estonia). Cadmium acetate and ammonium acetate were purchased from Sigma-Aldrich (St. Louis, MO). Tris(2-carboxyethyl)phosphine hydrochloride (TCEP-HCl) was obtained from Thermo Fisher Scientific (Rockford, IL). Deionized water (18.2 MΩ) was obtained from a Milli-Q water apparatus (Millipore, Billerica, MA).

Sample Preparation. ApoMT powder samples were prepared and stored using previously described procedures.[28] The sample was then reconstituted to 7 μM by 50 mM ammonium acetate (pH 7.4) solution containing 1 mM TCEP. ApoMT is prone to oxidation at physiological pH under aerobic conditions; thus, TCEP was added to maintain the cysteinyl thiols in the active reduced states. The metalation experiment was performed by sequential addition of 2, 4, and 6 μL of 1 mM cadmium acetate solution to 100 μL of a 7 μM apoMT solution. Following each addition of the Cd^{2+} solution, the protein was allowed to incubate for 1 h prior to MS measurements. Care was taken in all ESI-IM-MS experiments reported here to exclude ESI-induced protein oxidation and nonspecific metal binding as previously described.[28]

Ion Mobility Mass Spectrometry. ESI IM-MS measurements were performed on a Waters Synapt G2 HDMS instrument (Manchester, UK), a hybrid quadrupole/ion mobility (IM)/orthogonal time-of-flight mass spectrometer. The samples were analyzed as follows: 7 μM MT solutions were directly infused into the mass spectrometer at a 0.5 μL/min flow rate. ESI spectra were collected in the positive ion mode with a capillary voltage of 1.0−1.5 kV, sample cone voltage of 10 V, and extraction cone voltage of 1 V. The helium cell and nitrogen traveling wave (TW) regions were operated at 180 and 60 mL/min flows, respectively. A TW velocity of 300 m/s and TW height of 20 V were used for all the experiments unless specified otherwise. All mass spectra were calibrated externally using a solution of sodium iodide. CCS data were calibrated using ubiquitin cytochrome c and myoglobin as previously described.[42]

dx.doi.org/10.1021/ja5047878 | J. Am. Chem. Soc. 2014, 136, 9499−9508

Abundances of Cd_iMT^{n+} were determined by performing a baseline correction and calculating the area under the peaks. We also evaluated the effect of salt adducts by including them in the total abundance of Cd_iMT^{n+}. Since the salt adducts are present in all charge states detected, no significant difference was observed in the charge state distributions.

Ion arrival-time distribution (ATD) can be very sensitive to experimental parameters, especially experimental conditions that may alter the effective ion temperature (T_{eff}),[43−45] and this is especially apparent for apoMT and the partially metalated ions. To illustrate this point, ATDs for $apoMT^{5+}$ and Cd_7MT^{5+} are shown in the Supporting Information, Figure S1. Note that the CCS profiles differ significantly when using conditions that increase T_{eff}. Specifically, peaks corresponding to larger CCS peaks are observed in Figure S1A,C, but these peaks are attenuated or absent in data taken under conditions that minimize ion heating. All the IM-MS data reported herein were obtained under conditions where nitrogen gas flow and the voltages applied to the sample cone, extraction cone, and trap bias were adjusted to minimize ion heating, specifically instrument conditions that yield ATDs as shown in Figure S1B,D.

Molecular Dynamics Simulations. Due to the unavailability of the structure(s) for intact human MT-2A, structures from NMR of the separate domains[21] were connected (PDB: 1MHU and 2MHU) using a trans configuration (backbone dihedral angle $\omega \approx 180°$) between the two connecting lysines (Lys30-Lys31) as the starting structure for MD simulations of fully metalated Cd_7MT. Structures for partially metalated Cd_iMTs (i = 1−6) were generated by placing the Cd^{2+} ions in specific bonding sites, as indicated in Scheme 1, which shows the amino acid sequence of MT and the numbering scheme of Cd^{2+} assigned by NMR experiments.[21] Charges on the hydrophilic amino acid side chains, viz., the ε-amino groups of the lysines and the carboxylic acid side chains of aspartic acid and glutamic acid, were assigned assuming a pH of 7. That is, cadmium ion is 2+, cadmium-coordinated deprotonated cysteine is −1, lysine is +1, aspartic and glutamic acids are −1, and free cysteine and other amino acids are neutral. The overall charge state for each starting structure is provided in the Supporting Information. We note that there may be other possible Cd^{2+} configurations for the partially metalated forms. For example, Cd^{2+} may bind cysteines different from those designated in Scheme 1. In addition, the coordination number may not be equal to 4, as the preferred Cd^{2+} coordination can be either tetrahedral or octahedral.[46] For example, Cd^{2+} ions are octahedrally coordinated in carp parvalbumin, concanavalin A, thermolysin, and troponin C.[46] However, it is not clear how these variables should be treated because the structure, coordination number, and site occupancy for partially metalated MTs have not been determined experimentally. Therefore, the simulations are limited to previously reported Cd^{2+}−S bonding configurations in human Cd_7MT (Scheme 1).

Scheme 1. Sequence of Human MT-2A and Its Metal−Sulfur Connectivities[a]

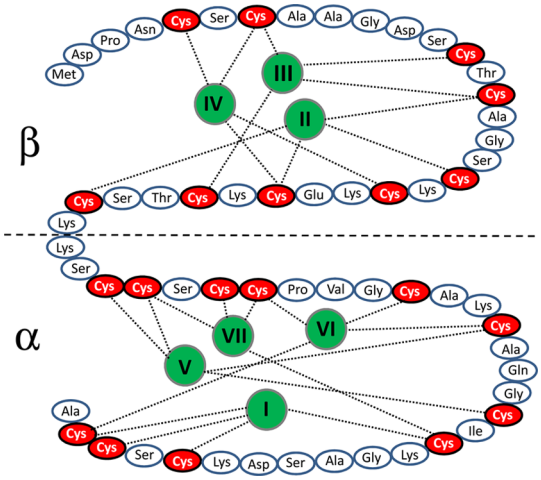

[a]The dotted lines denote the Cd^{2+}−Cys coordination. The Cd^{2+} ions are labeled I−VII using the cadmium−thiolate coordination derived from NMR studies.[21] The dashed line, α, and β denote the boundaries and locations of the two domains, respectively.

All-atom MD simulations were performed using the AMBER 9.0 FF99SB force field, which is extended to include parameters for cadmium−thiolate clusters (Table S1).[47] Solution-phase structures were simulated by using a modified generalized Born implicit solvent model (igb = 5)[48] to represent an aqueous solution environment. The initial structures were energy-minimized, followed by simulations at 300 K *in vacuo* (solvent-free) or implicit solvent model for 25 or 50 ns. "Dehydrated structures" were generated from solution-phase structures by using *in vacuo* energy minimization.[37,49−51] CCS calculations were carried out using a trajectory method implemented in MOBCAL,[52] in which the atomic energy and van der Waals radius of Cu^{2+} were used for Cd^{2+}. A complete description of the approach used for the simulations is provided in the Supporting Information. The distribution of CCSs for each simulation model is represented by a histogram with a 10 Å^2 interval. The simulated structures were clustered into families using a Cα root-mean-square deviation (RMSD)-based clustering algorithm in the MMTSB tool set.[53] Representative structures, determined as those closer to the centroid of each cluster, were selected to represent the candidate experimental structures.

RESULTS

The mechanism of metalation of human MT-2A by Cd^{2+} was previously studied by ESI-MS.[28] The ESI mass spectrum of apoMT contains abundant $apoMT^{n+}$ ions that range from n = 3 to 6, but the most abundant ion signals correspond to n = 4 and 5. Addition of aliquots of cadmium acetate solution to a solution of apoMT results in stepwise addition of Cd^{2+} to form Cd_iMT, where i ranges from 0 to 7 (Figure 1A; data for the full m/z range are shown in Figure S3).[28] A general concern with ESI-MS-based metal-binding studies is the possible occurrence of nonspecific interactions. The data indicate that nonspecific Cd^{2+} association is negligible. Cd^{2+} was shown to bind only to MT as the concentration of Cd^{2+} increases, and not to the non-MT species (impurities present in the original sample) that served as reference proteins (Figure S3).

The ESI charge state distribution of the Cd_iMT ions shows a dependence on the numbers of metal ions (Figure 1B), and such changes in charge state distribution could be linked to changes in solution-phase conformations that alter the solvent-accessible surface area (*vide infra*).[54,55] As the number of metal ions increases, the abundances of low charge state ions (n = 3 and 4) increase, whereas the abundances of high charge states ions (n = 5 and 6) decrease.

IM-MS provides a direct approach for monitoring the products of reaction (speciation) as well as conformational changes that occur upon addition of Cd^{2+} ions. Ion mobility CCS data for the Cd_iMT species are shown in Figure 1C; ATD data are provided in the Supporting Information, Figure S4. The CCS profiles for each of the charge states of apoMT span a wide range; viz., the 3+ and 4+ ions range from ∼700 to ∼800 Å^2, and the 5+ ions range from ∼730 to ∼1100 Å^2 (Figure 1C, top). We note that the peak widths for apo and partially metalated MT ions are substantially broad (drift time/peak width (DT/PW) ≈ 5.5, 5.2, and 2.7 for $apoMT^{n+}$ (n = 3−5), respectively; see Figure S4). This is indicative of an ion population composed of a high degree of conformational heterogeneity. In general, the CCS profile for each charge state becomes narrower and shifts to lower CCS values as the

dx.doi.org/10.1021/ja5047878 | J. Am. Chem. Soc. 2014, 136, 9499−9508

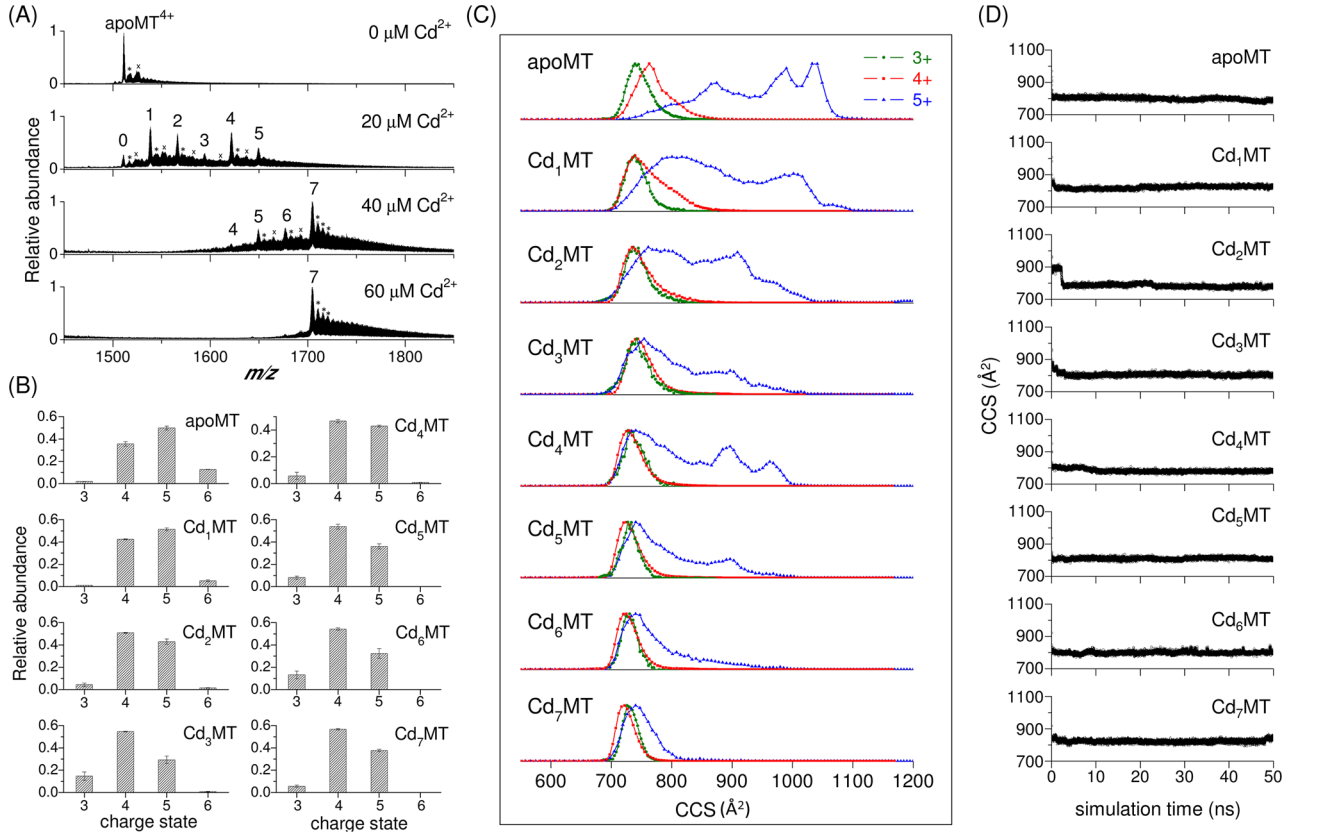

Figure 1. (A) ESI-MS spectra of a 7 μM apoMT solution (pH 7.4) and titration of apoMT with 20, 40, and 60 μM Cd^{2+}. Numbers above peaks denote the metal stoichiometry of the Cd_iMT species (i = 0−7). Data are shown for the m/z range of 4+ ions only. Additional peaks at +23 Da (*) and +60 Da (×) correspond to sodium and acetate adducts. The full ESI-MS spectrum is shown in Figure S3. (B) Charge state distributions of Cd_iMT (i = 0−7). Relative abundances were determined from the areas under the peaks after a baseline correction. (C) Overlay of CCS distributions of Cd_iMT as a function of metal accumulation. Three charge states observed from native electrospray ionization (50 mM ammonium acetate with 1 mM TCEP at pH 7.4) are shown in green (3+), red (4+), and blue (5+). Note all the CCS data were obtained using ion source and ion transfer conditions that minimize collisional heating,[43,44,77] which maximizes the preservation of native solution structures.[78,79] We also note that dimeric forms of fully metalated MT species (Cd_5Zn_2MT, Cd_7MT, and Zn_7MT) have been reported.[20,80,81] Although low-abundance dimer ions of partially and fully metalated forms (i = 1−7) were observed (6+ dimer ions, see Figure S4) under the experimental conditions used for this study, the discussion will be limited to the monomeric species. (D) Representative *in vacuo* MD simulations of Cd_iMT (i = 0−7). We have considered all possible metal ion binding configurations (or metal ion distributions) for each of the partially metalated forms (i = 1−6), except the case of i = 4. Data presented here represent one particular configuration with consecutive placement of the metal ions into the binding pockets in the order I → V → VII → VI → II → III → IV, the reverse of the demetalation order proposed by the Stillman group.[76] Detailed data for all other possible metal ion binding sites of Cd_iMT are provided in Figure S6. It is worth noting that the gas-phase simulations for other metal binding configurations do not yield significant differences in CCS values (see Figure S6).

number of metal ions increases (Figure 1C), indicating that addition of Cd^{2+} ions yields more-compact, ordered conformations. The reduction in conformational diversity and disorder accompanying metal ion addition is most pronounced for the Cd_iMT^{5+} ions. Note that the addition of a single Cd^{2+} ion narrows the peak profile and shifts the CCSs to smaller values, and subsequent addition of Cd^{2+} ions further narrows the CCS profile. The CCS values show a consistent decrease except for the case from i = 3 to 4, which will be addressed in the Discussion section. In general, for $i \leq 4$, multiple distinct conformations coexist and the population shifts to the compact conformers; however, for $i > 4$, the peak profiles become progressively narrower and primarily populate compact conformations. Collectively, the charge state distributions and CCS data show that metalation promotes a reduction in conformational diversity and yields compact conformations.

In an effort to understand detailed molecular features of the conformers observed in the IM-MS experiments, *in vacuo* MD simulations that yield conformations for solvent-free, gas-phase ions were performed. Independent of the number of metal ions added, the simulations of the candidate conformers have a relatively narrow CCS distribution centered at ~800 $Å^2$ (Figure 1D). Although the simulation data are in good agreement with those of the compact conformations (3+ and 4+ ions), the extended conformations (5+ ions) observed in the IM-MS experiments clearly show a more complicated metalation pathway (Figure 1C). Note that the features for these extended conformations remain undetected even when the temperature used for MD simulations is increased to 500 K (see Figure S5).

Ion mobility sample ions that have experienced dramatic changes in their local environments, i.e., ions in solution, are ejected as micrometer-size droplets which evaporate to yield nanometer-size droplets; finally, evaporation of remnant water molecules yields solvent-free gas-phase ions.[56] To aid in understanding the effects of desolvation on conformer preferences, simulations were carried out using implicit solvent (water) to yield solution-phase conformations. In an effort to mimic the ESI conditions, the water was removed from the MD

dx.doi.org/10.1021/ja5047878 | J. Am. Chem. Soc. 2014, 136, 9499−9508

solution-phase conformers, followed by energy minimization *in vacuo* to yield what is referred to as "dehydrated" conformers (see Figure 2A).[14,16,50] The differences between gas-phase and

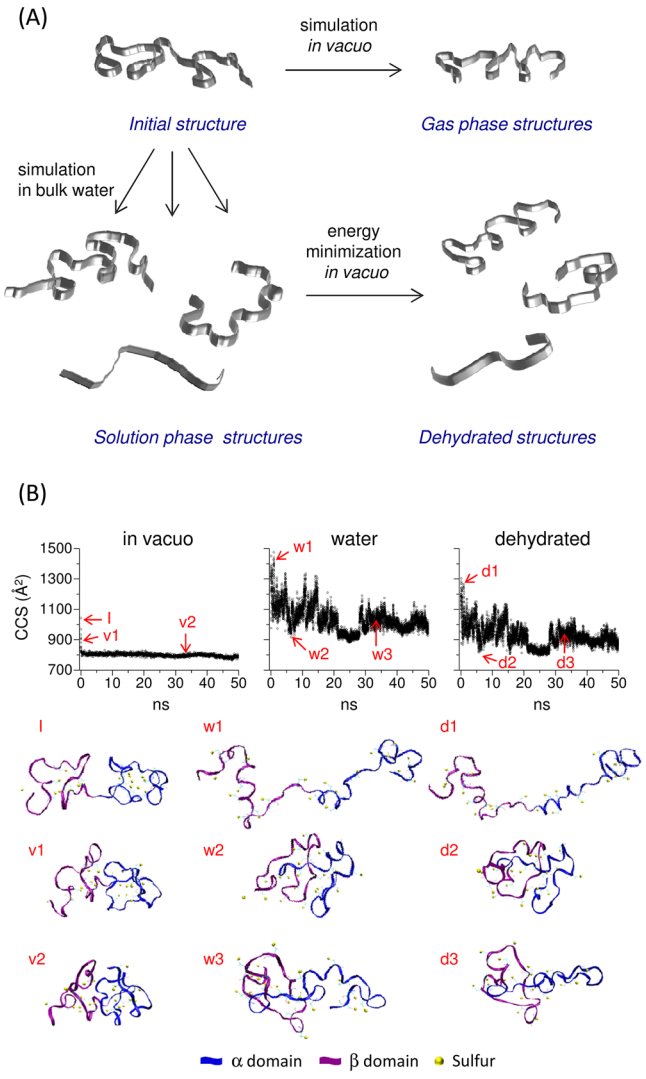

Figure 2. (A) Schematic representation of MD simulations in three models: *in vacuo*, implicit solvent (water), and dehydration. *In vacuo* simulations generate the gas-phase conformations, and implicit water simulations were used to generate solution-phase conformations. Subsequent dehydration from the solution-phase conformations was performed by energy minimization *in vacuo* to generate the dehydrated conformation. (B) MD simulations of apoMT. Structure I corresponds to the initial structure of apoMT obtained from the NMR structure (Cd_7MT) after removal of all metal ions. Trajectories v1 and v2 are snapshots after simulation *in vacuo* for 0.05 and 33.2 ns, respectively. Trajectories w1, w2, and w3 are time-evolution structures after 1.0, 6.5, and 33.2 ns in water. Trajectories d1, d2, and d3 are dehydrated structures from solution structures w1, w2, and w3, respectively.

dehydrated conformations are (1) whether the initial conformation is allowed to evolve in bulk water as opposed to a solvent-free environment, and (2) whether the energies of the conformations are being reduced in the simulation process. A comparison of simulation data in *vacuo*, in water, and upon subsequent dehydration for apoMT is presented in Figure 2B. The *in vacuo* simulation shows that the initial conformer rapidly (within 0.1 ns, trajectory v1) assumes a compact conformation that does not change significantly over the 50 ns sampling time frame (trajectory v2 represents the equilibrated conformation). Conversely, sample ions obtained from implicit water simulations have CCSs that range from 900 to 1500 Å^2, suggesting a wide range of conformers and/or a highly disordered ion population. The labels w1 and w2 represent oscillations between extended and compact conformations, and w3 represents a conformation having an intermediate size. "Dehydrated" conformations retain the general features of solution-phase ions, but the CCSs are somewhat smaller, indicating that the conformers "shrink" *in vacuo* owing to the loss of water (800−1300 Å^2).[49,50] The trajectories d1, d2, and d3 resemble the original solution conformers w1, w2, and w3, respectively, but the overall conformations are refined in vacuum. Skinner et al. and Silveira et al. recently reported on this phenomenon and showed that the "shrinkage" is the result of intramolecular charge solvation that occurs upon removal of the solvent.[56,57] This explanation is consistent with arguments that have been used previously to rationalize differences in experimental and calculated CCSs on the basis of XRD crystal and NMR structures.[49,58] Histograms of the CCSs for the dehydrated conformations of apoMT with formal charges are summarized in Figure 3A. Good agreement was obtained between the simulated conformational space (MD) and the range of conformer population (IM-MS). We note that effects of charge states for simulations of apoMT are small (data not shown). Simulations by manipulating charge states (protonation at Asp2, Asp11, Glu23, or Asp55) reveal similar structural fluctuation (open−close motions for solution-phase and dehydrated structures) and similar conformational space for dehydrated structures (800−1300 Å^2, data not shown).

MD simulations were used to examine conformational changes that accompany metal ion Cd^{2+} ion binding. The simulations were performed by adding Cd^{2+} ions to specific sites according to the numbering scheme as first proposed by Wüthrich (Scheme 1).[21] Our previous study clearly showed that Cd_4MT is a stable intermediate and that all four of the metal ions are located in the α-domain;[28] however, the Cd_4MT product represents the stable product of metalation, and its formation does not dictate that the initial metal ion addition is limited to the α-domain. Consequently, there remain ambiguities regarding metalation sequence and metal ion binding site(s) in partially metalated species, especially for the Cd_iMT (i = 1−3). As the apo and partially metalated MTs are proposed to be disordered, it is more likely that all the binding sites are exposed and accessible for metal binding. In addition, the broad range of CCSs for these partially metalated forms (Figure 1C) provides strong evidence for multiple conformers, which most likely differ in terms of metal ion binding sites. Although it is difficult to design experiments that unequivocally resolve such issues, it should be possible to probe this further by using MD simulations to generate candidate conformers for partially metalated Cd_iMT (i = 1−6) and compare predicted and experimentally measured CCSs.

Figure 3 contains data for conformers generated by simulation that have metal ions located in different domains and different binding sites. The complete set of simulation data is shown in the Supporting Information, Figure S6. The CCS distributions for dehydrated conformations span the range of 800−1200 Å^2 (Figure 3). These data show that a single metal ion configuration can adopt multiple conformational states. For example, for i = 1, the conformer with Cd^{2+} ion bound at site I yields two distinct populations of conformers (B, Figure 3). In addition, the conformers with Cd^{2+} bound in different binding

dx.doi.org/10.1021/ja5047878 | J. Am. Chem. Soc. 2014, 136, 9499−9508

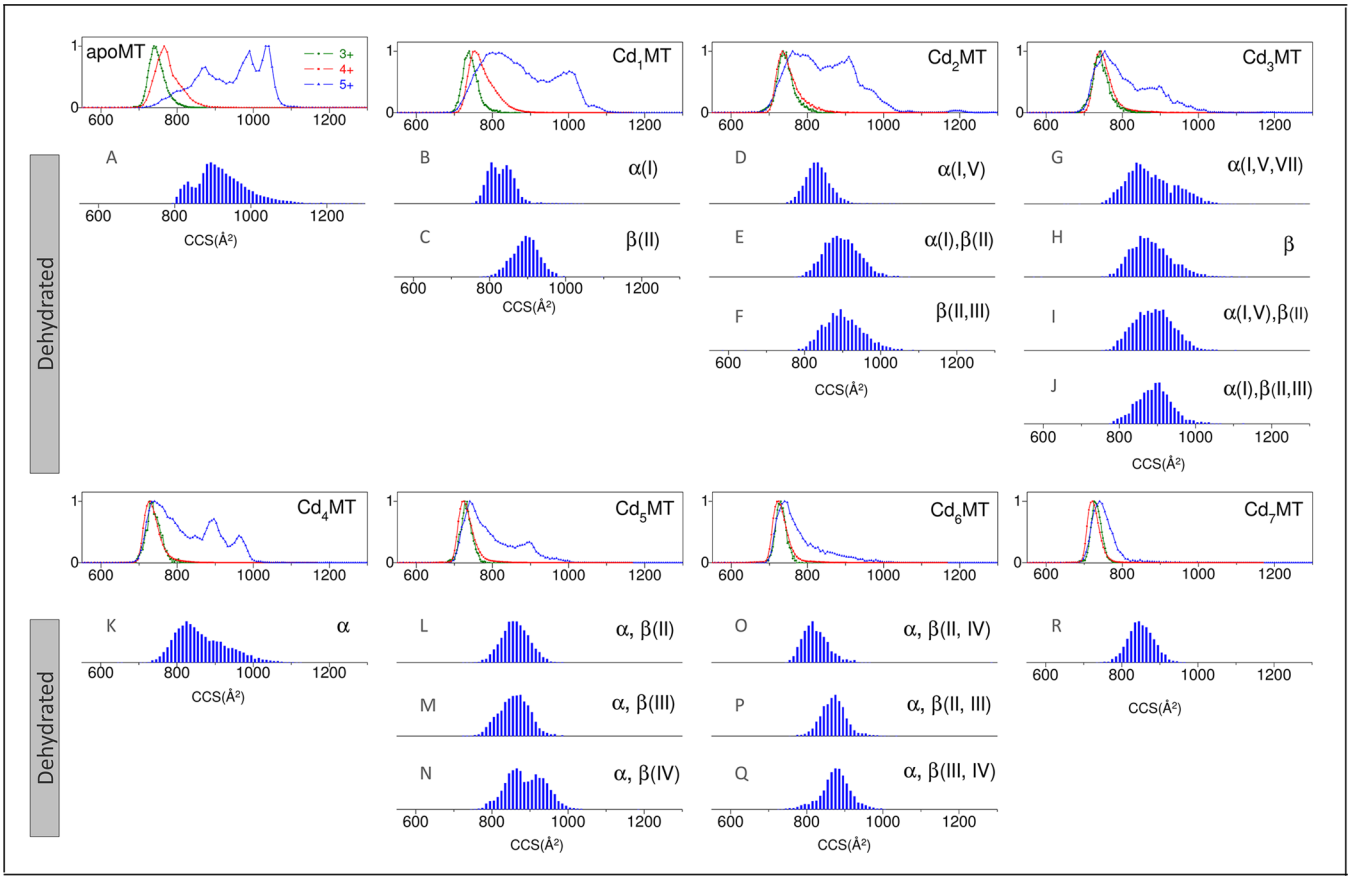

Figure 3. Histograms of CCSs for simulated dehydrated structures. Detailed simulation data are provided in Figure S6. The simulations were performed on 18 MT conformers (A–R) that have different metal ion compositions as well as different metal ion binding sites. The domain and specific location of metal ions are indicated on the right of the histograms. ESI-IM-MS data for the three charge states (3+, green; 4+, red; and 5+, blue) are shown above the histograms.

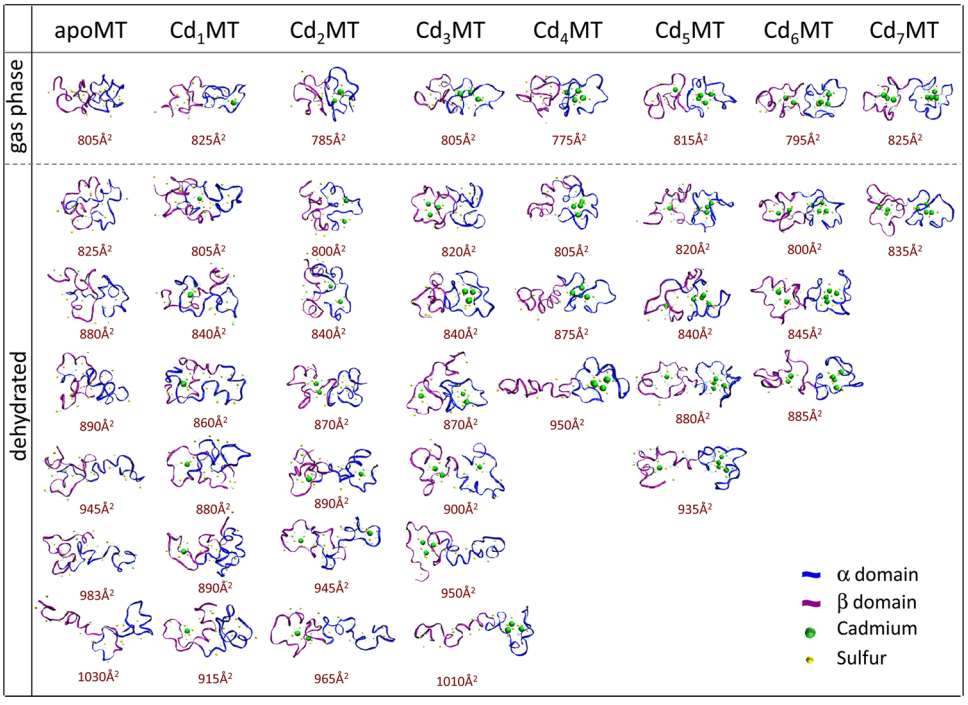

Figure 4. Representative structures of Cd_iMT (i = 0–7) in (A) gas phase and (B) solution phase. Numbers underneath the conformations correspond to the calculated CCS.

dx.doi.org/10.1021/ja5047878 | J. Am. Chem. Soc. 2014, 136, 9499–9508

sites can yield different conformational preferences; note that for i = 1, the B conformers have smaller CCSs than the C conformers (metal bound at site II). The difference in CCSs for Cd_iMTs with Cd^{2+} bound to different sites decreases as the number of metal ions increases; presumably the species having a greater number of bound metal ions are folded or partially folded, which limits the numbers of conformer states. That is, for i > 3, the conformers with different metal distributions yield smaller differences in their conformational states, and for i = 7, the CCS narrows to a single population.

The comparison between CCSs for MD-generated conformers and experimental CCSs suggests that the compact conformers observed in IM-MS experiments (Cd_iMT^{3+} and Cd_iMT^{4+} ions) agree quite well with the gas-phase conformers (Figure 1D) and/or the compact states of the dehydrated conformers (Figure 3), whereas the extended conformers (Cd_iMT^{5+} ions) agree best with the dehydrated conformers. Clearly, the simulations appear to overestimate the CCSs for the metalated forms, and the deviation increases as the number of the metal ions increases (max error <13%). Although not fully understood, the reason(s) for this discrepancy could be attributed to errors in calibration of traveling-wave CCS,[59] intrinsic errors in MD and MOBCAL calculation,[60] and most likely the parameters of d-block metal ion (Cd^{2+}) used in AMBER force field and trajectory method, which remains an underdeveloped area in MD simulations and CCS calculation.[61,62]

Figure 4 contains MD simulation-generated representative conformers for gas-phase and dehydrated Cd_iMT species (i = 0−7); detailed structural clusters and all representative conformations are provided in Figure S6. Although the gas-phase simulations favor compact conformations for all the Cd_iMT ions, the dehydrated simulations represent a broad range of conformer populations. For example, the simulation for apoMT yields six distinct conformations. The compact conformer (CCS ≈ 825 Å^2) matches a globular conformation, whereas the other conformers in the range of CCSs from 880 to 1030 Å^2 display a greater extent of unfolding. Binding of the metal ions promotes protein folding in the region around the metal ions, whereas other regions not involved in metal binding remain dynamic. Addition of a single Cd^{2+} ion yields globular-like conformers where the domain involved in metal binding appears to be partially folded while the other domain appears less ordered. Conformers of species with i = 2−3 are more ordered, but the majority of the protein backbone remains unstructured and dynamic. We note that the conformers with distinct structures may yield similar CCSs. For example, at i = 2, conformers with CCS = 945 and 965 Å^2 are clearly different in terms of metal ion configuration and protein structure. At i = 4, three representative conformers contain a fully folded α-domain with structural variation that arises from the extent of unfolding in the β-domains. In the case of i = 5−6, the region of interdomain linker remains disordered and results in several conformers that differ only in the projection of the α- and β-domains. At i = 7, the simulation yields a single conformation that corresponds to the well-known dumbbell-shaped structure.

DISCUSSION

IM-MS is now widely used for determination of CCSs and conformational heterogeneity of peptide/protein ions; however, there are few studies where the ion-neutral CCSs of native-like states are correlated to 3-D shapes and conformations generated by MD simulations.[37,45,51,58,63−65] An advantage of IM-MS is that it is a "label-free" methodology that can be used to characterize protein conformations and track conformational changes without need for intrinsic or external spectroscopic probes (fluorophore and secondary structures),[51,66] even proteins with conformational micro-heterogeneities including folding of an intrinsically disordered protein.[67] Most importantly, conformation information provided by IM-MS is molecule-specific, which permits the characterization of each metalated state in a dynamic, complex system.

The CCS profiles obtained from the centroid of the Cd_iMT^{3+} and Cd_iMT^{4+} ions are significantly smaller than that for the Cd_iMT^{5+}, and there may be multiple reasons for these differences. Although high charge states are subject to Coulombic repulsion that could result in increases in protein size and CCS, it is more likely that the CCS for the 5^+ charge state originates from disordered solution phase conformations.[55,68] That is, the solution conformers exhibiting lower solvent-accessible surface area (compact conformers) give rise to the lower charge states and smaller CCSs in gas phase, whereas the conformers having higher solvent accessible area (extended conformers) yield higher charge states and larger CCSs.

MD simulations suggest that apoMT shifts rapidly between extended and globular-like conformations in solution (Figure 2B). Further structural analysis on these simulated structures shows that all potential hydrogen bonds appear to be transient with <30% frequencies (Supporting Information, Table S2), suggesting that apoMT is highly dynamic and conformationally disordered in the bulk solution. Indeed, examination of the amino acid sequence of MT shows a compositional preference for small and hydrophilic amino acids and a lack of bulky hydrophobic and aromatic residues, which may prevent proteins from adopting a stable globular fold.[12] Complementary ESI techniques reveal similar structural information from hydrogen/deuterium exchange and proteolytic digestion, i.e., apoMT is rapidly digested (trypsin) to peptides within 5 min and nearly all hydrogens are exchanged instantly (data not shown). However, the above-mentioned methods do not provide information on conformation population. Ion mobility provides a direct measure for the conformational distribution; the IM-MS data suggest that apoMT comprises a highly heterogeneous ensemble that populates between CCS = 750 Å^2 (globular-like compact conformation) and 1050 Å^2 (coil-rich extended conformations, Figure 4). The data are consistent with the proposed disordered character of apoMT in solution, suggesting that the disorder features could be retained even in the absence of bulk water. This shows that IM-MS is capable of probing conformation population even for an "unstructured" protein.[37]

The simulation and experimental data for apoMT agree quite well in terms of the range of conformation population; however, these two sets of data do not show quantitative agreement with the overall CCS profiles, viz., the abundances of the numerous microstates (Figure 3A). The discrepancy can be explained as follows. The simulated profiles could be affected by the initial conformations, sampling methods, and length of sampling times used to generate solution-phase conformers and dehydrated conformations. Consequently, it is important to note that, although the MD simulations are very effective for protein conformation searches, they provide largely qualitative data and only serve as predictors for the possible conformations. That is, MD simulations are used to provide

dx.doi.org/10.1021/ja5047878 | J. Am. Chem. Soc. 2014, 136, 9499−9508

candidate conformations for the conformational states observed experimentally. On the other hand, the experimental CCS profiles represent a composite of a number of specific conformations that are formed by the ESI dehydration process and could also be complicated by some degree of collisional ion activation, even though great care was taken to sample the ions as gently as possible.

ESI charge-state distributions have been directly linked to solution-phase conformations because there is a strong correlation between observed charge states and solvent-accessible surface area.[54,55] Shifts in the charge-state distribution upon addition of Cd^{2+} ions to MT (Figure 1B) could be viewed as evidence that coordination of Cd^{2+} to MT induces conformational changes; however, IM-MS CCSs and MD simulations provide even stronger evidence of the metal-induced conformational changes. The CCS profiles (Figure 1C) show a marked shift to smaller values and reduction in peak width as the number of metal ions increases, implying that metalation favors more-compact, ordered conformations. Although apoMT shows a wide range of conformational states, binding of a single Cd^{2+} ion induces reduction in accessible surface area, as evidenced by changes in the charge-state distribution and protein ion size (decreased CCS). Subsequent addition of Cd^{2+} ions promotes further changes in charge-state distributions and reduction in protein ion size; however, the regions of the protein backbone that are not directly involved in metal binding remain disordered, as indicated by the peak tailing to higher CCS profiles.

It is somewhat surprising that the marked changes in CCS profiles are observed upon addition of a single Cd^{2+} ion (Figure 1C). Shifts in the CCS profiles for the stepwise addition of one, two, and three Cd^{2+} ions are indicative of formation of more compact conformers and an ion population that is composed of multiple conformational states. The comparison between experimental and theoretical CCSs (Figure 3) suggests that the broad ion populations for Cd_iMT (i = 1−3) are likely attributed not only to multiple conformational preferences of a single metal ion configuration but also to multiple conformers with different binding sites of metal ions. Our earlier study showed clear evidence that the metal ions of Cd_4MT are exclusively located in the α domain.[28] Therefore, it is highly probable that Cd^{2+} ions are initially bound to a number of sites and then shuttled to more thermodynamically stable sites. In addition, the CCS for the entire ion population shows a consistent decrease as the number of metal ions bound increases, except for the case from i = 3 to 4 (Figure 1C; abundances of conformers at CCS = 850−1000 Å^2 increase), which provides evidence for a distinct transition of conformation. Although the reason or reasons are not fully identified, the data could possibly be correlated to metal swapping to the α-domain (Cd_4MT) from conformations in which metal ions are present in both domains (Cd_3MT). This model suggests that the metalation mechanism of Cd^{2+} is probably similar to that of Co^{2+} proposed by Vasak and Petering.[69,70] We note that the proposed metalation model is derived from thermodynamic partially metalated products under equilibrated conditions, and thus it might be different from that based on the kinetic products.

In the case of i = 4, the α-domain is fully folded;[28] thus, the empty β-domain is most likely highly disordered. Indeed, the MD simulation suggests that the distinct conformations for Cd_4MT can be attributed to a different orientation of the β-domain (Figure 4). As Cd^{2+} ions bind to the β-domain, i.e., i = 5−6, the conformational heterogeneity decreases (CCS profiles become more narrow), indicative of formation of compact conformers. That is, the population or populations corresponding to conformers that have elongated interdomain linkers (CCS = 800−950 Å^2) decrease as the number of Cd^{2+} increases. At i = 7, both CCSs obtained from the IM-MS and MD narrow to a single population that is consistent with the previously suggested dumbbell-shaped structure.[21] Collectively, the data show that metal-induced folding of MT occurs through multiple pathways and involves disordered-to-ordered and extended-to-compact conformational transitions.

In addition to the conformation information provided by IMS/MD data, ESI-MS provides valuable information about relative stabilities for each metalated form.[28] We have previously reported the ratio of apparent binding constants for the stepwise metal-binding, K_1:K_2:K_3:K_4:K_5:K_6:K_7 = 15:3.0:1.0:16:3.2:1.0:3.9 for human MT-2A,[28] which indicates that Cd_4MT is a relatively stable intermediate. The relative distribution of the Cd_iMT observed in these experiments is different from that reported in Stillman's work, which proposed a non-cooperative manner of binding between Cd^{2+} and human MT-1A.[71,72] Although the reasons for this discrepancy are not fully identified, it could be attributed to slightly different sample preparation and ESI conditions used. In Stillman's work, samples were incubated under argon, and the capillary voltage used was 3−4.2 kV for ESI; in our study, samples were in the presence of TCEP, and ∼1−1.5 kV capillary voltage was used to minimize the possibility of ESI-induced oxidation. The discrepancy could also be due to different isoforms analyzed, as there is increasing awareness that the metal-binding properties of one isoform cannot be directly applied to other isoforms.[73] The IM-MS and MD simulations provide new information for understanding the metalation mechanism of MT-2A. The large value for K_1 is attributed to the disordered apoMT that presents solvent-exposed cysteinyl sulfur groups, thereby accelerating reactivity to metal ion(s). The decrease in values from K_1 to K_3 and from K_4 to K_6 is consistent with conformational changes that occur as the number of bound metals increases, in line with the model proposed by Stillman.[74] Specifically, the binding of metal ions induces protein folding and inverts the active cysteinyl sites from the protein surface to the protein interior.[74] These structural changes potentially relocate the remaining active cysteinyl sulfur groups, thereby decreasing their accessibility/reactivity toward incoming metal ions.[75,76] The sharp increase in K_4 is linked to a large-scale conformational change that accompanies metal ion rearrangement (swapping) that shifts the equilibrium from a less stable Cd_4MT (metal ions located in both domains) to a more stable conformation that has all four metal ions located in the α-domain.

■ CONCLUSION

Here, the first experimental data describing the effect of stepwise metalation on the conformation of human MT-2A are reported. The changes in ESI charge-state distribution for metal-free, partially metalated to fully metalated states are attributed to successive decreases in the solvent-accessible surface area. IM-MS and MD data clearly show that the metal-free protein is conformationally disordered and metalation yields compact and ordered conformations. The partially metalated forms populate multiple conformational states that reflect conformational multiplicity of the protein backbone that does not involve metal binding. It appears that initial metal ion binding occurs in both the α- and β-domains, but metal

swapping between the α- and β-domains ultimately yields the Cd_4MT product ions, where the metal ions are isolated to the α-domain.[28] MD simulations are consistent with metalation occurring along multi-trajectory pathways, with the final products corresponding to compact conformations; however, the partially metalated intermediates populate multiple conformational states. Both experimental and theoretical data support a metalation model where metal binding induces transitions from disordered-to-ordered and extended-to-compact conformations. This study provides, for the first time, experimental data and possible descriptions of conformations for the partially metalated MTs that could have a significant impact on the unknown conformational space in the protein folding landscape of MTs and serve as a model for other metalloproteins.

This study underscores the importance of IM-MS for mapping conformational changes of biologically important proteins that are not amenable to study by traditional structural techniques. An additional key component of this study is the importance of MD simulations for establishing the chemical/biological relevance of the experimental data. Most importantly, NMR and X-ray diffraction provide detailed structural information for a single metalated (fully metalated) Cd_7MT form, whereas the IM-MS/MD approach provides a global and dynamic view that shows a stepwise metal-induced conformational transition of an ensemble in terms of their 3° and 4° structures. It is anticipated that this approach could be applied to other complex systems that are highly dynamic and/or heterogeneous, viz., comprising multiple species and multiple conformations in solution.

■ ASSOCIATED CONTENT

Supporting Information

Detailed MD simulations and force field parameters for Cd^{2+} ions; evaluation of force field Cd^{2+} parameters by MD simulations of Cd_7MT in implicit water; hydrogen bond analysis of simulated structures for apoMT in bulk solution; IM-MS data for apo- and Cd_7MT^{5+} acquired in different instrumental parameters; full ESI-MS spectra of titration of apoMT by Cd^{2+}; ATDs of Cd_iMT^{n+} for different numbers of metal ion bound (i = 0−7) and charge state (n = 3−5); *in vacuo* MD simulations of apoMT at 300, 310, 320, 350, 400, 450, and 500 K; detailed MD simulation data for Cd_iMT (i = 0−7) at 300 K in gas phase, implicit solvent, dehydration models, and cluster structures for dehydrated structures. This material is available free of charge via the Internet at http://pubs.acs.org.

■ AUTHOR INFORMATION

Corresponding Author

russell@mail.chem.tamu.edu

Notes

The authors declare no competing financial interest.

■ ACKNOWLEDGMENTS

The IM-MS/MDS research was supported by the National Science Foundation (DBI-0821700 and CHE-0541587), the Robert A. Welch Foundation (A-1176) provided financial support for S.-H.C., and the fundamental IM-MS research was supported by the U.S. Department of Energy, Division of Chemical Sciences, BES (DE-FG02-04R15520). The efforts of Evamarie Capareda in preparation and editing of the manuscript are greatly appreciated.

■ REFERENCES

(1) Waldron, K. J.; Rutherford, J. C.; Ford, D.; Robinson, N. J. *Nature* **2009**, *460*, 823−830.
(2) Leal, S. S.; Botelho, H. M.; Gomes, C. M. *Coord. Chem. Rev.* **2012**, *256*, 2253−2270.
(3) Zou, J.; Kajita, K.; Sugimoto, N. *Angew. Chem., Int. Ed.* **2001**, *40*, 2274−2277.
(4) Yoshiike, Y.; Tanemura, K.; Murayama, O.; Akagi, T.; Murayama, M.; Sato, S.; Sun, X.; Tanaka, N.; Takashima, A. *J. Biol. Chem.* **2001**, *276*, 32293−32299.
(5) Uversky, V. N.; Li, J.; Fink, A. L. *J. Biol. Chem.* **2001**, *276*, 44284−44296.
(6) Bocharova, O. V.; Breydo, L.; Salnikov, V. V.; Baskakov, I. V. *Biochemistry* **2005**, *44*, 6776−6787.
(7) Golts, N.; Snyder, H.; Frasier, M.; Theisler, C.; Choi, P.; Wolozin, B. *J. Biol. Chem.* **2002**, *277*, 16116−16123.
(8) Cuajungco, M. P.; Goldstein, L. E.; Nunomura, A.; Smith, M. A.; Lim, J. T.; Atwood, C. S.; Huang, X.; Farrag, Y. W.; Perry, G.; Bush, A. I. *J. Biol. Chem.* **2000**, *275*, 19439−19442.
(9) Margoshes, M.; Vallee, B. L. *J. Am. Chem. Soc.* **1957**, *79*, 4813−4814.
(10) Blindauer, C. A. *J. Inorg. Biochem.* **2013**, *121*, 145−155.
(11) Klaassen, C. D.; Liu, J.; Choudhuri, S. *Annu. Rev. Pharmacol. Toxicol.* **1999**, *39*, 267−294.
(12) Blindauer, C. A.; Leszczyszyn, O. I. *Nat. Prod. Rep.* **2010**, *27*, 720−741.
(13) Gong, Y. H.; Elliott, J. L. *Exp. Neurol.* **2000**, *162*, 27−36.
(14) Meloni, G.; Faller, P.; Vasak, M. *J. Biol. Chem.* **2007**, *282*, 16068−16078.
(15) Meloni, G.; Sonois, V.; Delaine, T.; Guilloreau, L.; Gillet, A.; Teissie, J.; Faller, P.; Vasak, M. *Nat. Chem. Biol.* **2008**, *4*, 366−372.
(16) Namdarghanbari, M. A.; Bertling, J.; Krezoski, S.; Petering, D. H. *J. Inorg. Biochem.* **2014**, In press.
(17) Pattanaik, A.; Shaw, C. F., III; Petering, D. H.; Garvey, J.; Kraker, A. J. *J. Inorg. Biochem.* **1994**, *54*, 91−105.
(18) Yang, Y.; Maret, W.; Vallee, B. L. *Proc. Natl. Acad. Sci. U.S.A.* **2001**, *98*, 5556−5559.
(19) Petering, D. H.; Zhu, J.; Krezoski, S.; Meeusen, J.; Kiekenbush, C.; Krull, S.; Specher, T.; Dughish, M. *Exp. Biol. Med.* **2006**, *231*, 1528−1534.
(20) Robbins, A. H.; McRee, D. E.; Williamson, M.; Collett, S. A.; Xuong, N. H.; Furey, W. F.; Wang, B. C.; Stout, C. D. *J. Mol. Biol.* **1991**, *221*, 1269−1293.
(21) Messerle, B. A.; Schaffer, A.; Vasak, M.; Kagi, J. H.; Wüthrich, K. *J. Mol. Biol.* **1990**, *214*, 765−779.
(22) Schultze, P.; Worgotter, E.; Braun, W.; Wagner, G.; Vasak, M.; Kagi, J. H.; Wüthrich, K. *J. Mol. Biol.* **1988**, *203*, 251−268.
(23) Arseniev, A.; Schultze, P.; Worgotter, E.; Braun, W.; Wagner, G.; Vasak, M.; Kagi, J. H.; Wüthrich, K. *J. Mol. Biol.* **1988**, *201*, 637−657.
(24) Braun, W.; Vasak, M.; Robbins, A. H.; Stout, C. D.; Wagner, G.; Kagi, J. H.; Wüthrich, K. *Proc. Natl. Acad. Sci. U.S.A.* **1992**, *89*, 10124−10128.
(25) Gehrig, P. M.; You, C.; Dallinger, R.; Gruber, C.; Brouwer, M.; Kagi, J. H.; Hunziker, P. E. *Protein Sci.* **2000**, *9*, 395−402.
(26) Palumaa, P.; Eriste, E.; Njunkova, O.; Pokras, L.; Jornvall, H.; Sillard, R. *Biochemistry* **2002**, *41*, 6158−6163.
(27) Zaia, J.; Fabris, D.; Wei, D.; Karpel, R. L.; Fenselau, C. *Protein Sci.* **1998**, *7*, 2398−2404.
(28) Chen, S. H.; Russell, W. K.; Russell, D. H. *Anal. Chem.* **2013**, *85*, 3229−3237.
(29) Pearce, L. L.; Gandley, R. E.; Han, W.; Wasserloos, K.; Stitt, M.; Kanai, A. J.; McLaughlin, M. K.; Pitt, B. R.; Levitan, E. S. *Proc. Natl. Acad. Sci. U.S.A.* **2000**, *97*, 477−482.
(30) Hong, S. H.; Maret, W. *Proc. Natl. Acad. Sci. U.S.A.* **2003**, *100*, 2255−2260.
(31) Hong, S. H.; Hao, Q.; Maret, W. *Protein Eng. Des. Sel.* **2005**, *18*, 255−263.
(32) Liu, Y. L.; Lee, H. T.; Chang, C. C.; Kan, L. S. *Biochem. Biophys. Res. Commun.* **2003**, *306*, 59−63.

(33) Yu, X.; Wu, Z.; Fenselau, C. *Biochemistry* **1995**, *34*, 3377−3385.
(34) Yu, X.; Wojciechowski, M.; Fenselau, C. *Anal. Chem.* **1993**, *65*, 1355−1359.
(35) Zaia, J.; Jiang, L.; Han, M. S.; Tabb, J. R.; Wu, Z.; Fabris, D.; Fenselau, C. *Biochemistry* **1996**, *35*, 2830−2835.
(36) Hathout, Y.; Fabris, D.; Fenselau, C. *Int. J. Mass Spectrom.* **2001**, *204*, 1−6.
(37) Pierson, N. A.; Chen, L.; Valentine, S. J.; Russell, D. H.; Clemmer, D. E. *J. Am. Chem. Soc.* **2011**, *133*, 13810−13813.
(38) Breuker, K.; McLafferty, F. W. *Proc. Natl. Acad. Sci. U.S.A.* **2008**, *105*, 18145−18152.
(39) Vahidi, S.; Stocks, B. B.; Konermann, L. *Anal. Chem.* **2013**, *85*, 10471−10478.
(40) Nielson, K. B.; Winge, D. R. *J. Biol. Chem.* **1983**, *258*, 13063−13069.
(41) Guo, Y.; Ling, Y.; Thomson, B. A.; Siu, K. W. *J. Am. Soc. Mass Spectrom.* **2005**, *16*, 1787−1794.
(42) Ruotolo, B. T.; Benesch, J. L.; Sandercock, A. M.; Hyung, S. J.; Robinson, C. V. *Nat. Protoc.* **2008**, *3*, 1139−1152.
(43) Morsa, D.; Gabelica, V.; De Pauw, E. *Anal. Chem.* **2011**, *83*, 5775−5782.
(44) Rand, K. D.; Pringle, S. D.; Morris, M.; Engen, J. R.; Brown, J. M. *J. Am. Soc. Mass Spectrom.* **2011**, *22*, 1784−1793.
(45) Arcella, A.; Portella, G.; Ruiz, M. L.; Eritja, R.; Vilaseca, M.; Gabelica, V.; Orozco, M. *J. Am. Chem. Soc.* **2012**, *134*, 6596−6606.
(46) Rulisek, L.; Vondrasek, J. *J. Inorg. Biochem.* **1998**, *71*, 115−127.
(47) Ni, F. Y.; Cai, B.; Ding, Z. C.; Zheng, F.; Zhang, M. J.; Wu, H. M.; Sun, H. Z.; Huang, Z. X. *Proteins* **2007**, *68*, 255−266.
(48) Onufriev, A.; Bashford, D.; Case, D. A. *Proteins* **2004**, *55*, 383−394.
(49) Bernstein, S. L.; Wyttenbach, T.; Baumketner, A.; Shea, J. E.; Bitan, G.; Teplow, D. B.; Bowers, M. T. *J. Am. Chem. Soc.* **2005**, *127*, 2075−2084.
(50) Baumketner, A.; Bernstein, S. L.; Wyttenbach, T.; Bitan, G.; Teplow, D. B.; Bowers, M. T.; Shea, J. E. *Protein Sci.* **2006**, *15*, 420−428.
(51) Dupuis, N. F.; Wu, C.; Shea, J. E.; Bowers, M. T. *J. Am. Chem. Soc.* **2011**, *133*, 7240−7243.
(52) Mesleh, M. F.; Hunter, J. M.; Shvartsburg, A. A.; Schatz, G. C.; Jarrold, M. F. *J. Phys. Chem.* **1996**, *100*, 16082−16086.
(53) Feig, M.; Karanicolas, J.; Brooks, C. L., III *J. Mol. Graph. Modell.* **2004**, *22*, 377−395.
(54) Kaltashov, I. A.; Mohimen, A. *Anal. Chem.* **2005**, *77*, 5370−5379.
(55) Testa, L.; Brocca, S.; Grandori, R. *Anal. Chem.* **2011**, *83*, 6459−6463.
(56) Silveira, J. A.; Fort, K. L.; Kim, D.; Servage, K. A.; Pierson, N. A.; Clemmer, D. E.; Russell, D. H. *J. Am. Chem. Soc.* **2013**, *135*, 19147−19153.
(57) Skinner, O. S.; McLafferty, F. W.; Breuker, K. *J. Am. Soc. Mass Spectrom.* **2012**, *23*, 1011−1014.
(58) Pagel, K.; Natan, E.; Hall, Z.; Fersht, A. R.; Robinson, C. V. *Angew. Chem., Int. Ed.* **2013**, *52*, 361−365.
(59) Bush, M. F.; Hall, Z.; Giles, K.; Hoyes, J.; Robinson, C. V.; Ruotolo, B. T. *Anal. Chem.* **2010**, *82*, 9557−9565.
(60) Campuzano, I.; Bush, M. F.; Robinson, C. V.; Beaumont, C.; Richardson, K.; Kim, H.; Kim, H. I. *Anal. Chem.* **2012**, *84*, 1026−1033.
(61) Hu, L.; Ryde, U. *J. Chem. Theory Comput.* **2011**, *7*, 2452−2463.
(62) Sakharov, D. V.; Lim, C. *J. Comput. Chem.* **2009**, *30*, 191−202.
(63) Chen, L.; Chen, S.-H.; Russell, D. H. *Anal. Chem.* **2013**, *85*, 7826−7833.
(64) Ruotolo, B. T.; Giles, K.; Campuzano, I.; Sandercock, A. M.; Bateman, R. H.; Robinson, C. V. *Science* **2005**, *310*, 1658−1661.
(65) Jurneczko, E.; Cruickshank, F.; Porrini, M.; Clarke, D. J.; Campuzano, I. D.; Morris, M.; Nikolova, P. V.; Barran, P. E. *Angew. Chem., Int. Ed.* **2013**, *52*, 4370−4374.
(66) Chen, L.; Gao, Y. Q.; Russell, D. H. *J. Phys. Chem. A* **2012**, *116*, 689−696.
(67) Canon, F.; Ballivian, R.; Chirot, F.; Antoine, R.; Sarni-Manchado, P.; Lemoine, J.; Dugourd, P. *J. Am. Chem. Soc.* **2011**, *133*, 7847−7852.
(68) Grabenauer, M.; Wyttenbach, T.; Sanghera, N.; Slade, S. E.; Pinheiro, T. J.; Scrivens, J. H.; Bowers, M. T. *J. Am. Chem. Soc.* **2010**, *132*, 8816−8818.
(69) Bertini, I.; Luchinat, C.; Messori, L.; Vasak, M. *J. Am. Chem. Soc.* **1989**, *111*, 7296−7300.
(70) Ejnik, J.; Robinson, J.; Zhu, J.; Forsterling, H.; Shaw, C. F.; Petering, D. H. *J. Inorg. Biochem.* **2002**, *88*, 144−152.
(71) Sutherland, D. E.; Summers, K. L.; Stillman, M. J. *Biochem. Biophys. Res. Commun.* **2012**, *426*, 601−607.
(72) Sutherland, D. E.; Stillman, M. J. *Biochem. Biophys. Res. Commun.* **2008**, *372*, 840−844.
(73) Palumaa, P.; Tammiste, I.; Kruusel, K.; Kangur, L.; Jornvall, H.; Sillard, R. *Biochim. Biophys. Acta* **2005**, *1747*, 205−211.
(74) Ngu, T. T.; Easton, A.; Stillman, M. J. *J. Am. Chem. Soc.* **2008**, *130*, 17016−17028.
(75) Rigby Duncan, K. E.; Stillman, M. J. *J. Inorg. Biochem.* **2006**, *100*, 2101−2107.
(76) Rigby, K. E.; Chan, J.; Mackie, J.; Stillman, M. J. *Proteins* **2006**, *62*, 159−172.
(77) Merenbloom, S. I.; Flick, T. G.; Williams, E. R. *J. Am. Soc. Mass Spectrom.* **2012**, *23*, 553−562.
(78) Dupuis, N. F.; Wu, C.; Shea, J. E.; Bowers, M. T. *J. Am. Chem. Soc.* **2009**, *131*, 18283−18292.
(79) Balthasart, F.; Plavec, J.; Gabelica, V. *J. Am. Soc. Mass Spectrom.* **2013**, *24*, 1−8.
(80) Zangger, K.; Armitage, I. M. *J. Inorg. Biochem.* **2002**, *88*, 135−143.
(81) Hathout, Y.; Reynolds, K. J.; Szilagyi, Z.; Fenselau, C. *J. Inorg. Biochem.* **2002**, *88*, 119−122.